

THE DISPERSION OF FAST RADIO BURSTS FROM A STRUCTURED INTERGALACTIC MEDIUM AT REDSHIFTS $Z < 1.5$

J. MICHAEL SHULL AND CHARLES W. DANFORTH
CASA, Department of Astrophysical & Planetary Sciences,
University of Colorado, Boulder, CO 80309
Draft version February 5, 2022

ABSTRACT

We analyze the sources of free electrons that produce the large dispersion measures, $DM \approx 300 - 1600$ (in units $\text{cm}^{-3} \text{ pc}$), observed toward fast radio bursts (FRBs). Individual galaxies typically produce $DM \sim 25 - 60 \text{ cm}^{-3} \text{ pc}$ from ionized gas in their disk, disk-halo interface, and circumgalactic medium. Toward an FRB source at redshift z , a homogeneous IGM containing a fraction f_{IGM} of cosmological baryons will produce $DM = (935 \text{ cm}^{-3} \text{ pc}) f_{\text{IGM}} h_{70}^{-1} I(z)$, where $I(z) = (2/3\Omega_m)[\{\Omega_m(1+z)^3 + \Omega_\Lambda\}^{1/2} - 1]$. A structured IGM of photoionized Ly α absorbers in the cosmic web produces similar dispersion, modeled from the observed distribution, $f_b(N, z)$, of H I (Ly α -forest) absorbers in column density and redshift with ionization corrections and scaling relations from cosmological simulations. An analytic formula for $DM(z)$ applied to observed FRB dispersions suggests that $z_{\text{FRB}} \approx 0.2 - 1.5$ for an IGM containing a significant baryon fraction, $f_{\text{IGM}} = 0.6 \pm 0.1$. Future surveys of the statistical distribution, $DM(z)$, of FRBs identified with specific galaxies and redshifts can be used to calibrate the IGM baryon fraction and distribution of Ly α absorbers. Fluctuations in DM at the level $\pm 10 \text{ cm}^{-3} \text{ pc}$ will arise from filaments and voids in the cosmic web.

Subject headings: cosmological parameters — observations — intergalactic medium — radio continuum: stars

1. INTRODUCTION

Of unknown origin, but suspected to arise in explosive events at extragalactic distances, fast radio bursts (FRBs) are radio pulses of milli-second duration that exhibit considerable dispersion in frequency (Lorimer et al. 2007; Thornton et al. 2013). The observed range of dispersion measures, $DM \equiv \int n_e dl \approx 300 - 1600 \text{ cm}^{-3} \text{ pc}$ (Petroff et al. 2016) corresponds to column densities of intervening electrons $N_e \approx (1 - 5) \times 10^{21} \text{ cm}^{-2}$. Most FRBs are isolated events, with the exception of the repeating FRB 121102 (Spitler et al. 2016) which was identified with a low-metallicity dwarf galaxy at $z = 0.193$ (Tendulkar et al. 2017; Bassa et al. 2017). This object has $DM = 557 \pm 2 \text{ cm}^{-3} \text{ pc}$ (Scholz et al. 2016), far larger than expected from the modeled distribution ($DM \sim 25 - 60$) of free electrons within the Milky Way (Cordes & Lazio 2002; Yao et al. 2017). These large dispersions could arise from the “circumburst medium”, from the host galaxy, or from the intergalactic medium (IGM).

In this paper, we argue that the most plausible source of the high dispersions are the large reservoirs of ionized gas in the IGM. The cosmological “missing baryons problem” (Fukugita et al. 1998) has largely been solved through spectroscopic observations of diffuse baryons using UV absorption lines toward quasars. These data and astrophysical analysis (Shull et al. 2012) show that the low-redshift IGM still contains a substantial fraction, $f_{\text{IGM}} \approx 0.5 - 0.7$, of the cosmological baryons, distributed in warm photoionized gas (Ly α forest at $T \approx 10^4 \text{ K}$) and a hotter, collisionally ionized medium ($T \approx 10^{5-7} \text{ K}$).

Thus, substantial dispersion of FRB pulses is naturally expected from ionized gas (H^+ and He^{+2}) that accompanies the intergalactic H I (Ly α) and metal-line absorption systems observed toward active galactic nuclei (AGN).

In Section 2, we assess the contributions to DM from intervening galaxies, including their extended gaseous halos and circumgalactic medium (CGM). Typical galactic halos produce $DM \sim 25 - 60 \text{ cm}^{-3} \text{ pc}$, consistent with the column density of free electrons, $N_e \approx 10^{20} \text{ cm}^{-2}$, observed in the warm ionized gas layer at the disk-halo interface of the Milky Way (Reynolds 1991; Gaensler et al. 2008). We then compute the integrated column density of electrons, N_e , from a homogeneous IGM that contains a substantial fraction, f_{IGM} , of the cosmological baryons. We derive an analytic formula to estimate the FRB redshift from the inferred IGM dispersion, DM_{IGM} and an assumed f_{IGM} . Finally, we calculate the distribution of $N_e(z)$ and $DM(z)$ from a spatially structured medium: the “cosmic web” of dark matter and baryon filaments. Our calculation is based on the observed distribution of low-redshift H I and metal-line absorbers from recent IGM surveys (Danforth & Shull 2008; Danforth et al. 2016; Shull et al. 2017) with the Cosmic Origins Spectrograph (Green et al. 2012) aboard the *Hubble Space Telescope* (*HST*).

The observed H I absorbers span a wide range of column densities, $N_{\text{HI}} (\text{cm}^{-2})$ between $12.5 < \log N_{\text{HI}} < 22.0$. The nomenclature of these systems includes the Lyman limit systems (LLS with $\log N_{\text{HI}} \geq 17.2$) and partial Lyman-limit systems (pLLS with $\log N_{\text{HI}} \approx 16.0 - 17.2$), and the much rarer “damped Ly α absorbers” (DLAs with $\log N_{\text{HI}} \geq 20.3$). For optically thin absorbers with $\log N_{\text{HI}} < 17.5$, large amounts of ionized hydrogen ac-

company the H I. Because the Ly α absorbers are highly photoionized by the metagalactic background from AGN (Haardt & Madau 2012), the neutral hydrogen absorption probes only a small fraction of the total plasma. In addition, the weak Ly α absorbers with $\log N_{\text{HI}} < 13$ are quite plentiful, with an absorption-line frequency per unit redshift, $dN/dz > 100$ along sight lines toward background quasars. Thus, the contribution of Ly α -forest absorbers to $N_e(z)$ is substantial and more uniform across the sky.

By analyzing the photoionization conditions in these H I absorbers, we calculate the column densities of free electrons per H I absorber. We then combine the H I absorber distribution with scaling relations of baryon overdensity (Δ_b) and gas temperature (T) with N_{HI} inferred from cosmological simulations to calculate $N_e(z)$ for a spatially structured IGM. From the scaling relations, we show that H I absorbers produce a flat distribution in integrated $N_e(z)$ over the range $12.5 \leq \log N_{\text{HI}} \leq 16.0$. We expect a turnover and fluctuations in the DM distribution at $\log N_{\text{HI}} > 15.5$, owing to the scarcity ($dN/dz < 1$) of strong H I absorbers. Future FRB surveys that localize the bursts and identify them with galaxies (with redshifts) can be used to model the IGM structure and to confirm the predicted large fraction of cosmological baryons in diffuse intergalactic structures.

2. ESTIMATES OF DISPERSION MEASURES

2.1. *Electrons in the Milky Way Halo Gas*

The observed dispersion measures toward Galactic pulsars are a standard method for modeling the spatial distribution of electrons within the Milky Way (Cordes & Lazio 2002). Coupled with observations of diffuse H α emission, these data have led to a model of diffuse ionized gas within a kpc of the Galactic disk. This ionized medium at the disk-halo interface is often called the “Reynolds Layer” and has a column density of free electrons $N_e \approx 10^{20} \text{ cm}^{-2}$. From pulsar surveys, this ionized layer has been fitted by various surveys to an exponential density distribution, $n_e(z) = n_0 \exp(-z/h)$, with mid-plane densities $n_0 \approx 0.019\text{--}0.035 \text{ cm}^{-3}$ and vertical scale heights $h \approx 880\text{--}950 \text{ pc}$ (Taylor & Cordes 1993; Cordes & Lazio 2002). Gaensler et al. (2008) made a joint analysis of pulsar dispersions and diffuse H α emission and found $n_0 \approx 0.014 \pm 0.001 \text{ cm}^{-3}$ and $h = 1830_{-250}^{+120} \text{ pc}$. Savage & Wakker (2009) obtained a revised exponential scale height $h = 1410_{-210}^{+260} \text{ pc}$. More recent analyses take into account spiral structure, multiple components (thin and thick Galactic disks, clumps, cavities). The product of mid-plane density and scale height yields the “perpendicular DM” integrated from the midplane to infinity. In the above models (Taylor & Cordes 1993; Cordes & Lazio 2002; Gaensler et al. 2008; Savage & Wakker 2009) the vertically integrated DM is 16.5, 33.0, 25.6 and 21.9 ($\text{cm}^{-3} \text{ pc}$) respectively.

The most recent model of the spatial distribution of Galactic free electrons (Yao et al. 2017) is based on 189 pulsars with independently measured distances. The thick disk component has mid-plane density $n_0 \approx 0.01132 \pm 0.00043 \text{ cm}^{-3}$ and scale height $h = 1673 \pm 53 \text{ pc}$, corresponding to vertically integrated $n_0 h = 18.9 \pm 0.9 \text{ cm}^{-3} \text{ pc}$. Their Table 14 applies their model to estimate redshifts for 17 FRBs from inferred IGM disper-

sions after subtracting modeled contributions from the Galaxy and a standard value, $\text{DM}_{\text{host}} = 100 \text{ cm}^{-3} \text{ pc}$, for the host galaxy. For 13 of the 17 FRBs, the modeled Galactic contribution ranges from $\approx 23\text{--}76 \text{ cm}^{-3} \text{ pc}$; four sources at low Galactic latitude have higher values.

2.2. *Electrons in Circumgalactic and Halo Gas*

The best estimates of ionized gas in the low Galactic halo come from column densities N of highly ionized interstellar metal-line absorbers toward O-type stars at high Galactic latitude ($b > 40^\circ$) and toward extragalactic sources such as AGN and blazars. By fitting $N \sin b$ versus elevation above the disk, using UV resonant absorption lines of abundant metal ions such as C IV, Si IV, and O VI, several groups (Sembach & Savage 1992; Shull & Slavin 1994) found vertical scale heights (2-5 kpc). The integrated column densities through the Galactic plane allow one to estimate the total column density of ionized hydrogen, after correcting the metal ions for ionization fraction and metallicity. The largest metal-ion column densities come from X-ray absorption studies (Nicastro et al. 2002; Yao & Wang 2005; Wang et al. 2005; Fang et al. 2006; Anderson & Bregman 2010) of the helium-like ion state of oxygen (O VII) and its K α line at 21.602 Å. Because O VII maintains a high ionization fraction, f_{OVII} , over a wide range of temperatures, $5.5 < \log T < 6.3$, in collisional ionization equilibrium, it provides the best sensitivity to hot coronal gas. Galactic absorption lines of O VIII and Ne IX and weaker lines from ions of O, Ne, C, and N have also been detected in selected AGN sight lines (Nicastro et al. 2016; Nevalainen et al. 2017).

The O VII absorption lines at $z \approx 0$ observed toward many AGN are interpreted as arising from coronal gas in the Galactic halo (Collins et al. 2006; Fang et al. 2006; Bregman 2007). Typical O VII column densities through the halo are $\log N_{\text{OVII}} \approx 16.0\text{--}16.3$, with some uncertainty owing to line saturation. For fully ionized gas with mean integrated column density $\langle N_{\text{OVII}} \rangle = (10^{16} \text{ cm}^{-2}) N_{16}$ and oxygen abundance $(\text{O}/\text{H}) = (4.9 \times 10^{-4}) Z_{\text{O}}$ relative to its solar value $(\text{O}/\text{H})_{\odot} = 4.9 \times 10^{-4}$, we find $N_e = (2.4 \times 10^{19} \text{ cm}^{-2}) N_{16} (f_{\text{OVII}} Z_{\text{O}})^{-1}$ corresponding to $\text{DM} = (7.7 \text{ cm}^{-3} \text{ pc}) N_{16} (f_{\text{OVII}} Z_{\text{O}})^{-1}$. With assumptions about the ionization and metallicity factors ($f_{\text{OVII}} Z_{\text{O}}$), the above papers estimate column densities of ionized hydrogen, $N_{\text{HI}} \approx 10^{20} \text{ cm}^{-2}$ ($\text{DM} \sim 30$) associated with the O VII absorption.

Strong O VI absorption lines in the ultraviolet (1032 and 1038 Å) have also been used to probe hot gas in the halos of external galaxies. The COS-Halos survey (Tumlinson et al. 2011) of the CGM of galaxy halos intercepted by a sight line toward a background AGN found mean O VI column densities $\langle N_{\text{OVI}} \rangle \approx 10^{14.5} \text{ cm}^{-2}$ for actively star-forming galaxies. Employing corrections for metallicity (O/H) and O VI ionization fraction, $f_{\text{OVI}} \approx 0.2$ in collisional ionization equilibrium, we estimate a column density of ionized gas (and electrons) of $N_e \approx (3.2 \times 10^{18} \text{ cm}^{-2}) Z_{\text{O}}^{-1}$. At the metallicities ($Z_{\text{O}} = 0.1\text{--}0.5$) observed in Galactic high-latitude high-velocity clouds (Wakker et al. 1999; Shull et al. 2009; Fox et al. 2014) the disk-halo interface gas traced by O VI produces dispersions $\text{DM} \sim 5\text{--}10 \text{ cm}^{-3} \text{ pc}$. The frequencies per unit redshift of galaxy halos, LLS,

DLAs, and other strong absorbers are too low to explain the large FRB dispersions. For example, the incidence of LLS at $z \leq 0.5$ has been measured by *HST*/COS (Shull et al. 2017) to be $(dN/dz)_{\text{LLS}} = 0.36_{-0.13}^{+0.20}$. If each LLS contributed $N_e \approx 10^{17.5} \text{ cm}^{-2}$, the mean integrated dispersion would be $\langle \text{DM} \rangle \approx 0.04 \text{ cm}^{-3} \text{ pc}$ toward FRBs at $z \approx 1$. Similarly, if intervening galactic halos and their CGM each produce $\text{DM} \sim 30 - 50 \text{ cm}^{-3} \text{ pc}$, an FRB sight line would need to intercept 10-30 such galaxies to accumulate sufficient electron column densities sufficient to explain the large FRB dispersions, $\text{DM} = 300 - 1600 \text{ cm}^{-3} \text{ pc}$. For all these reasons, we now explore dispersion in the the baryon-rich IGM.

2.3. Electrons in a Homogeneous IGM

As a first estimate of the IGM dispersion, we compute the integrated column density of electrons in a homogeneous IGM, whose mass density increases as $(1+z)^3$ with redshift. The mean cosmological baryon density has been well constrained by measurements of the primordial D/H ratio (Cooke et al. 2016) and the acoustic spectrum of the cosmic microwave background (Planck Collaboration 2016). The cosmological baryon density is independent of the Hubble constant $H_0 = (100 \text{ km s}^{-1} \text{ Mpc}^{-1})h$ and its scaling factor (h), $\bar{\rho}_b = \Omega_b \rho_{\text{cr}} = 4.17 \times 10^{-31} \text{ g cm}^{-3}$, based on $\Omega_b h^2 = 0.02217$ and a critical (closure) density $\rho_{\text{cr}} = (1.879 \times 10^{-29} \text{ g cm}^{-3})h^2$. With a primordial helium abundance $Y \approx 0.2449$ by mass (Aver et al. 2013), this mass density corresponds to a number density of hydrogen,

$$\bar{n}_H = \frac{\rho_b(1-Y)}{m_H} \approx (1.88 \times 10^{-7} \text{ cm}^{-3})f_{\text{IGM}}(1+z)^3, \quad (1)$$

where $f_{\text{IGM}} \approx 0.5 - 0.7$ is the likely fraction of diffuse baryons in the IGM (Shull et al. 2012). The number density of electrons is $\bar{n}_e = 1.167\bar{n}_H$, accounting for H^+ and He^{+2} ,

To find the column density, N_e , of electrons toward a source at redshift z , we use the relationship between proper length and redshift in a flat Λ CDM cosmology,

$$\frac{d\ell}{dz} = \frac{c}{H_0}(1+z)^{-1} [\Omega_m(1+z)^3 + \Omega_\Lambda]^{-1/2}. \quad (2)$$

Here, we adopt $\Omega_m \approx 0.3$ and $\Omega_\Lambda \approx 0.7$ as the fractional contributions of matter and dark energy to closure density and $H_0 = (70 \text{ km s}^{-1} \text{ Mpc}^{-1})h_{70}$. The integrated column density of electrons out to redshift z is then

$$\begin{aligned} N_e(z) &= (1.167)(1.87 \times 10^{-7} \text{ cm}^{-3})f_{\text{IGM}}\frac{c}{H_0} \\ &\times \int_0^z \frac{(1+z)^2 dz}{[\Omega_m(1+z)^3 + \Omega_\Lambda]^{1/2}} \\ &= (2.88 \times 10^{21} \text{ cm}^{-2})f_{\text{IGM}} h_{70}^{-1} I(z). \end{aligned} \quad (3)$$

The redshift integral can be done analytically,

$$\begin{aligned} I(z) &= \int_0^z \frac{(1+z)^2 dz}{[\Omega_m(1+z)^3 + \Omega_\Lambda]^{1/2}} \\ &= \frac{2}{3\Omega_m} \left[\{\Omega_m(1+z)^3 + \Omega_\Lambda\}^{1/2} - 1 \right], \end{aligned} \quad (4)$$

with values of 0.686, 1.69, and 2.94 at $z = 0.5, 1.0, 1.5$ respectively. For a homogeneous IGM, the dispersion measure can be expressed as

$$\text{DM} = (935 \text{ cm}^{-3} \text{ pc})f_{\text{IGM}} h_{70}^{-1} I(z). \quad (5)$$

We invert this relation for $I(z)$ to find an analytic formula for the FRB redshift based on the inferred dispersion, DM_{IGM} , contributed by the IGM,

$$(1+z) = \left[\frac{\{(3\Omega_m d/2) + 1\}^2 - \Omega_\Lambda}{\Omega_m} \right]^{1/3}. \quad (6)$$

Here, we have defined the dimensionless dispersion parameter

$$d = \left[\frac{\text{DM}_{\text{IGM}} h_{70}}{(935 \text{ cm}^{-3} \text{ pc})f_{\text{IGM}}} \right]. \quad (7)$$

Table 1 gives our estimated redshifts for these 17 FRBs and 8 others from recent papers (Bhandari et al. 2017; Bannister et al. 2017; Caleb et al. 2017). We use equations (6) and (7) with values of IGM baryon fraction, $f_{\text{IGM}} = 0.6 \pm 0.1$, consistent with *HST*/COS baryon surveys and cosmological simulations (Shull et al. 2012). For the IGM dispersion, we follow the methodology in Yao et al. (2017) in which $\text{DM}_{\text{IGM}} = \text{DM}_{\text{obs}} - \text{DM}_{\text{Gal}} - \text{DM}_{\text{Host}}$. We use their model of the electron distribution within the Milky Way for the Galactic contribution, DM_{Gal} , and we adopt a constant dispersion $\text{DM}_{\text{Host}} = 100 \text{ cm}^{-3} \text{ pc}$ (their assumption) for the FRB host galaxy. This assumption is uncertain, as DM_{Host} is larger than most values within the Milky Way. For 17 FRBs in their study, Yao et al. (2017) inferred redshifts ranging from $z = 0.238$ to $z = 2.059$ with median $z = 0.687$. The median modeled IGM dispersion is $490 \text{ cm}^{-3} \text{ pc}$ (range 170 to $1469 \text{ cm}^{-3} \text{ pc}$) and the median observed dispersion is $776 \text{ cm}^{-3} \text{ pc}$ (range 375 to $1629 \text{ cm}^{-3} \text{ pc}$). In general, our method produces lower redshifts for the 17 FRBs, ranging from $z = 0.254_{-0.032}^{+0.043}$ for the burst with the lowest dispersion ($\text{DM}_{\text{IGM}} \approx 170 \text{ cm}^{-3} \text{ pc}$) to $z = 1.38_{-0.147}^{+0.196}$ for the largest dispersion ($\text{DM}_{\text{IGM}} \approx 1469 \text{ cm}^{-3} \text{ pc}$). The error bars on these redshifts are propagated from the assumed uncertainty in IGM baryon fraction. They do not include errors in the cosmological parameters (Ω_m , Ω_Λ , H_0) or assumptions about the subtracted portions of DM from the Galaxy or FRB host galaxy.

2.4. Electrons Associated with the Ly α Forest

Next, we compute the electrons associated with a more realistic, structured IGM based on the distribution of Ly α absorbers measured in recent surveys. Figure 1 shows examples of low-redshift H I absorbers in the spectra of four blazars. From a recent survey with *HST*/COS (Danforth et al. 2016), the typical frequency per unit redshift of H I absorbers is $dN/dz \approx 50 - 150$ for weak systems in the Ly α forest ($\log N_{\text{HI}} \approx 12.5 - 14.0$). A survey of higher column density absorbers (Shull et al. 2017) characterized the distribution of low-redshift LLS ($\log N_{\text{HI}} \geq 17.2$) and pLLS ($\log N_{\text{HI}} \approx 16.0 - 17.2$). These absorbers are considerably rarer, with $(dN/dz)_{\text{LLS}} \approx 0.36_{-0.13}^{+0.20}$ and $(dN/dz)_{\text{pLLS}} \approx 1.69 \pm 0.23$.

To compute the ionized gas (and electrons) associated with these Ly α absorbers, we employ scaling re-

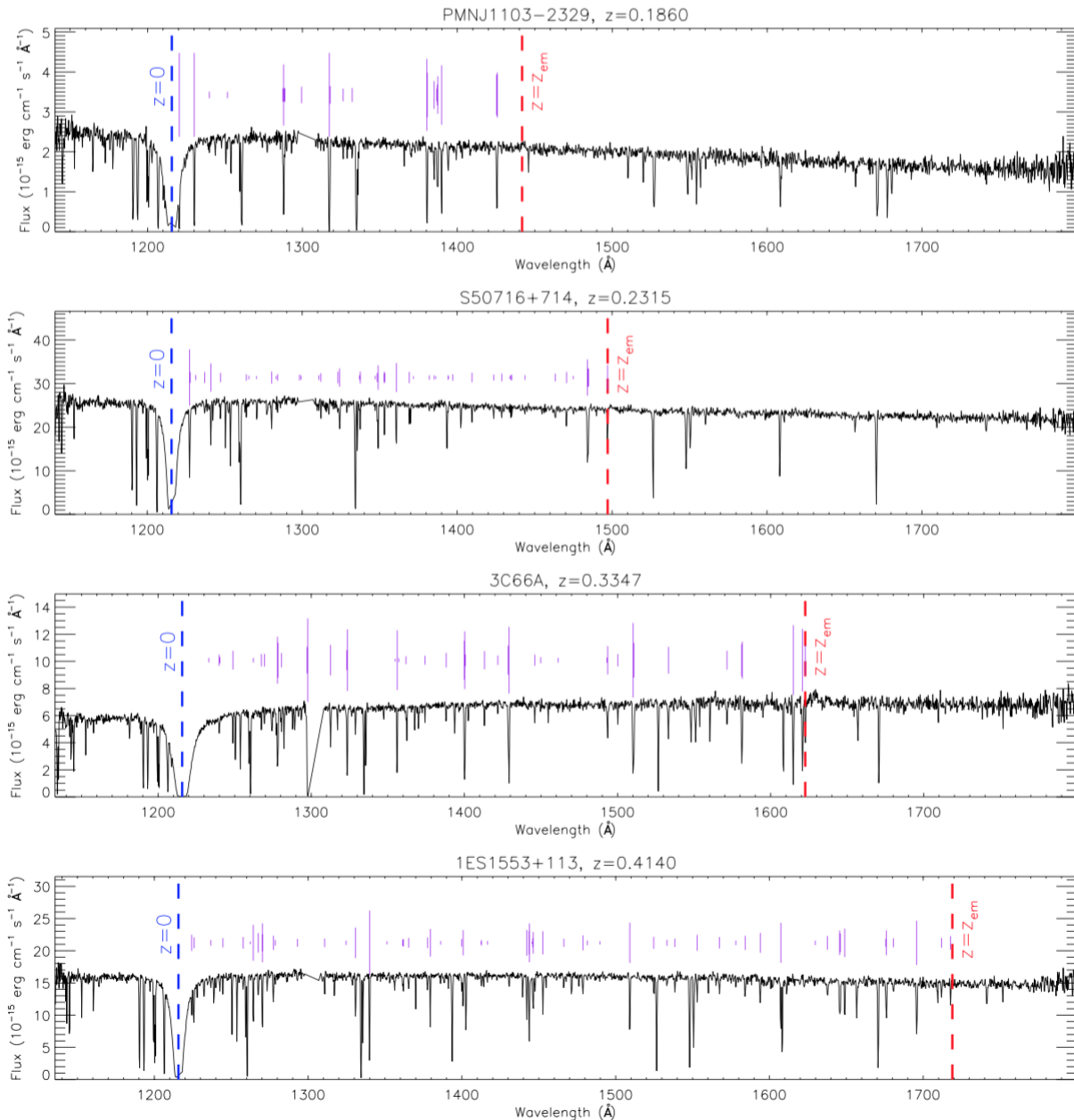


FIG. 1.— HST/COS spectra of the low-redshift H I (Ly α) absorbers toward four blazars at $z = 0.1860$ (PMN J1103-2329), $z = 0.2315$ (S5 0716+714), $z = 0.3347$ (3C 66A), and $z \approx 0.414$ (1ES 1553+113). The redshift of PG 1553+113 (Danforth et al. 2010) was inferred statistically from the wavelength at which no further Ly α lines are seen. Tick marks above the continuum indicate intervening Ly α absorbers, with length denoting the H I column density.

lations found in simulations of the low-redshift IGM. These formulae allow us to relate the baryon overdensity of an absorber, $\Delta_b = \rho_b/\bar{\rho}_b$, to H I column density $N_{\text{HI}} = (10^{14} \text{ cm}^{-3})N_{14}$ and gas temperature T . The relations are expressed as power laws,

$$\Delta_b = (36.9)N_{14}^\alpha \quad \text{and} \quad T = (5000 \text{ K})\Delta_b^\beta. \quad (8)$$

In our IGM simulations (Shull et al. 2015) we found $\alpha \approx 0.65$ and $\beta \approx 0.60$. This temperature relation has been confirmed by other groups, although several simulations found slightly larger values of $\alpha = 0.741 \pm 0.003$ (Davé

et al. 2010), 0.786 ± 0.001 (Tepper-Garcia et al. 2012), and 0.770 ± 0.022 (Gaikwad et al. 2017). Baryon overdensity is defined relative to the mean (co-moving) cosmological baryon density, $\bar{\rho}_b = \Omega_b \rho_{\text{cr}} = 4.17 \times 10^{-31} \text{ g cm}^{-3}$. For an H I absorber at redshift z and overdensity Δ_b , the hydrogen number density is

$$n_H(z) = \frac{\rho_b(1-Y)}{m_H}(1+z)^3 \approx (1.88 \times 10^{-7} \text{ cm}^{-3})\Delta_b(1+z)^3. \quad (9)$$

We assume that the plasma in this absorber is in photoionization equilibrium with the metagalactic ioniz-

ing background, with hydrogen photoionization rate Γ_H (s^{-1}) and the low-density (case-A) hydrogen recombination rate coefficient $\alpha_H^{(A)}$ ($\text{cm}^3 \text{s}^{-1}$). In the approximation $x_{\text{HI}} \ll 1$, the hydrogen neutral fraction is given by

$$x_{\text{HI}} = \frac{n_{\text{HI}}}{n_H} \approx \frac{n_e \alpha_H^{(A)}}{\Gamma_H}. \quad (10)$$

We approximate $\Gamma_H \approx (4.6 \times 10^{-14} \text{ s}^{-1})(1+z)^{4.4}$ for the hydrogen photoionization rate over the range $0 < z < 0.47$ (Shull et al. 2015) and adopt $\alpha_H^{(A)} \approx (4.09 \times 10^{-13} \text{ cm}^3 \text{ s}^{-1})T_4^{-0.726}$ at temperature $T = (10^4 \text{ K})T_4$. From $T(\Delta_b)$ and $\Delta_b(N_{14})$ in equation (8), we find

$$\begin{aligned} x_{\text{HI}} &\approx (3 \times 10^{-6})\Delta_b^{0.564}(1+z)^{-1.4} \\ &\approx (2.29 \times 10^{-5})N_{14}^{0.37}(1+z)^{-1.4}. \end{aligned} \quad (11)$$

The total column density of ionized hydrogen accompanying the H I is

$$N_{\text{H}} \approx \frac{N_{\text{HI}}}{x_{\text{HI}}} \approx (4.4 \times 10^{18} \text{ cm}^{-2})N_{14}^{0.63}(1+z)^{1.4}, \quad (12)$$

with a characteristic absorber size

$$L \approx \frac{N_{\text{HI}}}{n_H x_{\text{HI}}} \approx (200 \text{ kpc})N_{14}^{-0.02}(1+z)^{-1.6}, \quad (13)$$

nearly constant with H I column density. These scaling relations suggest that, at fixed redshift, higher column density absorbers have larger neutral fractions. The higher redshift absorbers are smaller and more ionized.

We now integrate the electron column densities over the distribution of H I absorbers found in the recent *HST*/COS surveys (Danforth et al. 2016; Shull et al. 2017). As shown in Figure 2, a power-law fit to the differential distribution in H I column density per unit redshift is $f(N, z) \equiv (d^2\mathcal{N}/dN_{\text{HI}}dz) \approx 50N_{14}^{-1.65}(1+z)^\gamma$. We adopt a redshift-evolution factor, $\gamma \approx 1.24$, from a new fit to the absorbers with $\log N_{\text{HI}} \geq 15$ (Danforth et al. 2016), and multiply by a factor of 1.167 for the electrons donated from He^{+2} . After the He II reionization epoch at $z \approx 2.7 - 3.2$, Ly α forest clouds have far more He^{+2} than He^+ (Shull et al. 2010). We arrive at the electron column density, $N_e(z)$, out to redshift z , integrated over column densities from $N_1 = 10^{12.5}$ to $N_2 = 10^{16.0} \text{ cm}^{-2}$,

$$\begin{aligned} N_e(z) &= (1.083)(4.4 \times 10^{18} \text{ cm}^{-2})(50) \\ &\times \int_0^z (1+z)^\gamma dz \int_{N_1}^{N_2} N_{14}^{-0.02} dN_{14} \\ &= (1.65 \times 10^{21} \text{ cm}^{-2}) \frac{[(1+z)^{\gamma+1} - 1]}{(\gamma+1)}. \end{aligned} \quad (14)$$

This column density translates to $\text{DM} = (534 \text{ cm}^{-3} \text{ pc})(\Delta z)_{\text{eff}}$, where the effective redshift accounts for the $(1+z)^\gamma$ evolution of the Ly α absorber frequency with redshift. For $\gamma = 1.24$, we have $(\Delta z)_{\text{eff}} = 0.66$ out to $z = 0.5$ and 1.66 out to $z = 1.0$. Additional baryons reside in the WHIM probed by O VI and Broad Ly α Absorbers.

3. SUMMARY AND DISCUSSION

Many physical locations have been suggested to explain the large pulse dispersions observed toward FRBs. In the

most recent DM model for the Galactic electron distribution (Yao et al. 2017) the Milky Way typically contributes $\text{DM} \sim 25 - 75 \text{ cm}^{-3} \text{ pc}$, consistent with other measurements of ionized gas. Studies of metal ions at the disk-halo interface and Galactic halo find electron column densities $N_e \approx 10^{20} \text{ cm}^{-3}$ ($\text{DM} \sim 30$). Thus, for the observed FRB range, $\text{DM} \approx 300 - 1600 \text{ cm}^{-3} \text{ pc}$, the host galaxy and the IGM are probably the dominant contributors to the dispersion. Yao et al. (2017) adopted a standard contribution, $\text{DM}_{\text{Host}} = 100 \text{ cm}^{-3} \text{ pc}$, from the host galaxy. After subtracting the modeled Galactic DM, they attribute the residual DM to plasma in the IGM. Their values for DM_{IGM} are in good agreement with values derived in Sections 2.3–2.4. It would be difficult for FRBs at cosmological distances to avoid having large dispersions, given the substantial baryon fractions inferred to reside in the IGM (Shull et al. 2012). For example, the Ly α forest likely contains 30% of the cosmic baryons in a warm (10^4 K) photoionized phase. Absorption from high ions such as O VI and Ne VIII (and broad Ly α absorbers) suggest a similar contribution from hotter gas ($10^5 - 10^7 \text{ K}$) in a phase called the WHIM (warm-hot intergalactic medium).

The agreement between estimates of cosmological dispersion measures, $\text{DM}(z)$, and baryon measurements from UV spectroscopic surveys, provides additional evidence that the IGM contains a substantial fraction, $f_{\text{IGM}} > 0.5$, of diffuse baryons. However, both are model-dependent estimates. One important prediction of our calculation is the flat contribution to $\text{DM}(z)$ from Ly α -forest absorbers across a wide range of column densities, $12.5 < \log N_{\text{HI}} < 16$. Further progress in using FRBs as IGM probes will require identifying their host galaxies and obtaining redshifts. One can then assemble a statistical sample to relate $\text{DM}(z)$ to electrons and H I absorbers in the IGM. Fluctuations in DM from a structured IGM are expected at the level of $\pm 10 \text{ cm}^{-3} \text{ pc}$ from the (Mpc-scale) filaments and (10-30 Mpc) voids produced by gravitational instability (Davé & Oppenheimer 2010; Smith et al. 2011). We also expect to see fluctuations at the level of $\text{DM} \approx 25 \text{ cm}^{-3} \text{ pc}$, owing to the scarcity of H I absorbers with $\log N > 15$. Our recent *HST*/COS survey (Shull et al. 2017) of strong Ly α absorbers ($0.24 < z < 0.48$) found line frequencies $(dN/dz) \approx 1.69 \pm 0.23$ at $\log N_{\text{HI}} \geq 16.0$ and $(dN/dz) \approx 4.95 \pm 0.39$ at $\log N_{\text{HI}} \geq 15.0$.

We now summarize the main results of our survey:

1. The large observed dispersions, $\text{DM} \approx 300 - 1600 \text{ cm}^{-3} \text{ pc}$, of FRB pulses are unlikely to arise in the ionized gaseous layers of galaxies or in their halos, but the integrated dispersion of electrons in the IGM naturally produces such values. For a homogeneous IGM containing a fraction f_{IGM} of cosmological baryons, the average dispersion measure $\text{DM} \approx (935 \text{ cm}^{-3} \text{ pc})f_{\text{IGM}}h_{70}^{-1}I(z)$, where $I(z) = (2/3\Omega_m)[\{\Omega_m(1+z)^3 + \Omega_\Lambda\}^{1/2} - 1]$.
2. Our model for $\text{DM}_{\text{IGM}}(z)$ provides a convenient analytic formula for estimating FRB redshifts, $(1+z) = \Omega_m^{-1/3} [\{(3\Omega_m d/2) + 1\}^2 - \Omega_\Lambda]^{1/3}$. The dimensionless parameter $d = [\text{DM}_{\text{IGM}} h_{70}/(935 \text{ cm}^{-3} \text{ pc})f_{\text{IGM}}]$ depends on

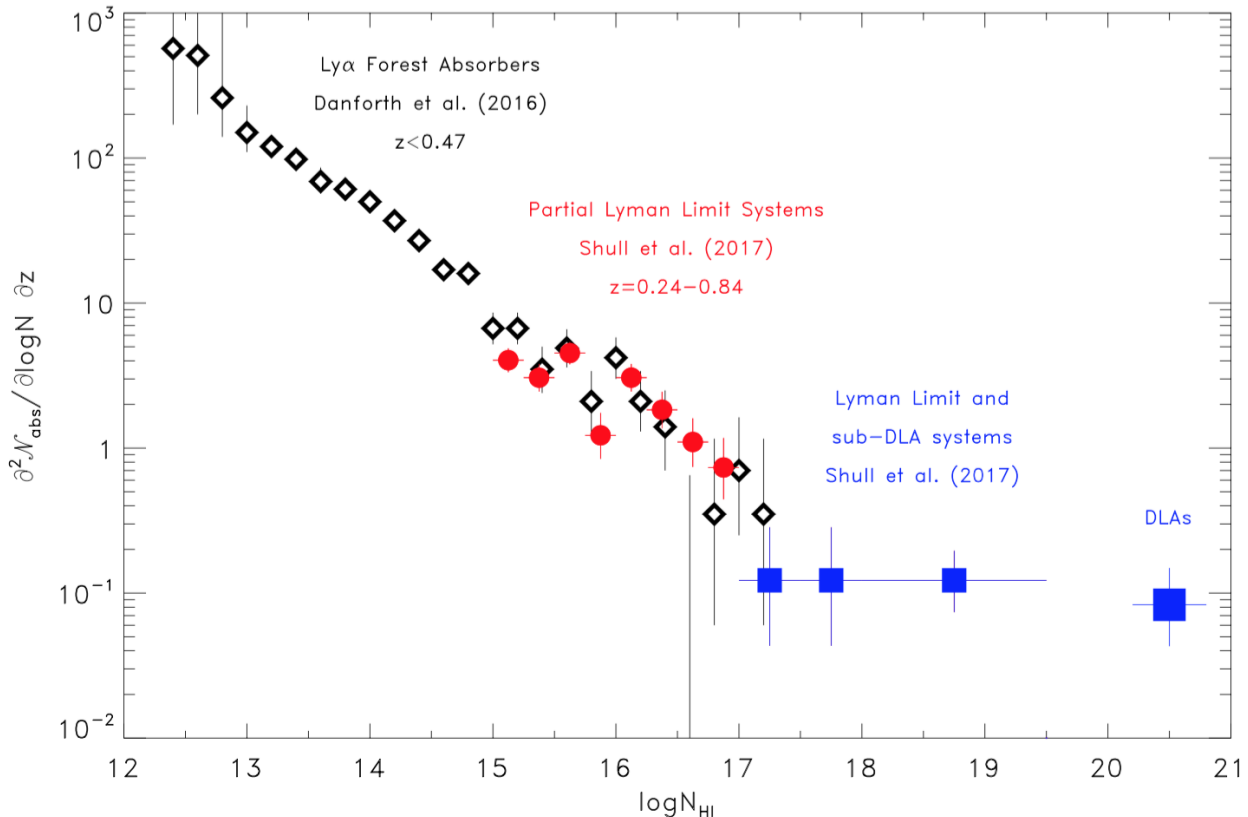


FIG. 2.— Distribution of low-redshift H I absorbers per unit redshift and column density ($\log N_{\text{HI}}$). Solid diamonds (black) are from the *HST*/COS survey (Danforth et al. 2016) of Ly α forest at $0 < z < 0.47$. Filled circles (red) are results from the *HST*/COS survey (Shull et al. 2017) of strong H I absorbers at $0.24 < z < 0.84$ (pLLS) and $0.24 < z < 0.48$ (LLS). The four solid squares (blue) show values for sub-DLA and DLA systems ($0 < z < 0.48$). The distribution of Ly α -forest absorbers is well fitted with a differential distribution, $f(N, z) \propto N^{-\beta}$, with $\beta = 1.65 \pm 0.02$.

- the dispersion attributed to the IGM, after subtracting contributions from the Milky Way and FRB host galaxy.
3. We also analyzed a more sophisticated IGM model using UV spectroscopic observations of the bivariate distribution ($d^2\mathcal{N}/dz dN_{\text{HI}}$) of intergalactic H I absorbers in column density and redshift, together with scaling relations from cosmological simulations of H I column densities with baryon overdensity, temperature, and ionization state. This model finds $\text{DM} \approx (534 \text{ cm}^{-3} \text{ pc})(\Delta z)_{\text{eff}}$ over effective pathlength $(\Delta z)_{\text{eff}} = 0.66$ integrated out to $z = 0.5$ and 1.66 to $z = 1.0$, consistent with $f_{\text{IGM}} \approx 0.6$.
 4. Our model of a structured IGM, together with scaling relations, predicts nearly equal contributions to the integrated DMs across a wide range of H I column densities, $12.5 \leq \log N < 16$. One expects fluctuations at the level of $\text{DM} \approx 25 \text{ cm}^{-3} \text{ pc}$ from absorbers $\log N_{\text{HI}} > 15.5$, when the number of strong absorbers per unit redshift drops below $d\mathcal{N}/dz < 1$.

5. With a sufficiently large sample of FRBs identified with galaxies (and redshifts) one can calibrate the fraction of baryons in the diffuse IGM. Strong filaments and voids in the cosmic web would appear as weak DM fluctuations at the level of $10 \text{ cm}^{-3} \text{ pc}$.

The IGM data originated from individual and survey observations of AGN taken with the Cosmic Origins Spectrograph on the *Hubble Space Telescope*. We appreciate helpful discussions with Jeremy Darling, Shri Kulkarni, and John Stocke. In early stages, this research was supported by grants HST-GO-13301.01.A and HST-GO-13302.01.A from the Space Telescope Science Institute to the University of Colorado Boulder. More recent work was carried out through academic support from the University of Colorado.

REFERENCES

- Anderson, M., & Bregman, J. N. 2010, *ApJ*, 714, 320
- Aver, E., Olive, K. A., & Skillman, E. D. 2013, *JCAP*, 11, 017
- Bannister, K. W., Shannon, R. M., Macquart, J.-P., et al. 2017, *ApJ*, 841, L12
- Bassa, C. G., Tendulkar, S. P., Adams, E. A. K., et al. 2017, *ApJ*, 834, L7
- Bhandari, S., Keane, E. F., Barr, E. D., et al. 2017, *MNRAS*, in press (arXiv:1711.08110)
- Bregman, J. N. 2007, *ARA&A*, 45, 221
- Caleb, M., Flynn, C., Bailes, M., et al. 2017, *MNRAS*, 468, 3746
- Collins, J. A., Shull, J. N., & Giroux, M. L. 2006, *ApJ*, 723, 196
- Cooke, R. J., Pettini, M., Nollett, K. M., & Jorgenson, R. 2016, *ApJ*, 830, 148
- Cordes, J. M., & Lazio, T. J. W. 2002, NE2001 Model of Galactic Distribution of Free Electrons and Fluctuations, arXiv preprint (astro-ph/0207156)
- Danforth, C. W., & Shull, J. M. 2008, *ApJ*, 679, 194
- Danforth, C. W., Keeney, B. A., Stocke, J. T., Shull, J. M., & Yao, Y. 2010, *ApJ*, 720, 976
- Danforth, C. W., Keeney, B. A., Tilton, E. M., et al. 2016, *ApJ*, 817, 111
- Davé, R., Oppenheimer, B. D., Katz, N., et al. 2010, *MNRAS*, 408, 2051
- Fang, T., McKee, C. F., Canizares, C. R., & Wolfire, M. 2006, *ApJ*, 644, 174
- Fox, A. J., Wakker, B.P., Barger, K. A., et al. 2014, *ApJ*, 787, 147
- Fukugita, M., Hogan, C. W., & Peebles, P. J. E. 1998, *ApJ*, 503, 518
- Gaensler, B. M., Madsen, G. J., Chatterjee, S., & Mao, S. A. 2008, *PASA*, 25, 184
- Gaikwad, P., Khaire, V., Choudhury, T. R. & Srianand, R. 2017, *MNRAS*, 466, 836
- Green, J. C., Froning, C. S., Osterman, S., et al. 2012, *ApJ*, 744, 60
- Haardt, F., & Madau, P. 2012, *ApJ*, 746, 125
- Lorimer, D., Bailes, M., McLaughlin, M., Narkevic, D., & Crawford, F. 2007, *Science*, 318, 777
- Nevalainen, J., Wakker, B., Kaastra, J., et al. 2017, *A&A*, 605, A47
- Nicastro, F., Senatore, F., Gupta, A., et al. 2016, *MNRAS*, 457, 676
- Nicastro, F., Zezas, A., Drake, H., et al. 2002, *ApJ*, 573, 157
- Petroff, E., Barr, E. D., Jameson, A., et al. 2016, *PASA*, 33, e045
- Planck Collaboration, et al. 2016, *A&A*, 594, A13
- Reynolds, R. J. 1991, *ApJ*, 372, L17
- Savage, B. D., & Wakker, B. P. 2009, *ApJ*, 702, 1472
- Scholz, P., Spitler, L. G., Hessels, J. W. T., et al. 2016, *ApJ*, 833, 177
- Sembach, K. R., & Savage B. D. 1992, *ApJS*, 83, 147
- Shull, J. M., Danforth, C. W., Tilton, E. M., Moloney, J., & Stevans, M. L. 2017, *ApJ*, 849, 106
- Shull, J. M., France, K., Danforth, C. W., Smith, B., & Tumlinson, J. 2010, *ApJ*, 722, 1312
- Shull, J. M., Jones, J. R., Danforth, C. W., & Collins, J. A. 2009, *ApJ*, 699, 754
- Shull, J. M., Moloney, P., Danforth, C. W., & Tilton, E.M. 2015, *ApJ*, 811, 3
- Shull, J. M., & Slavin, J. D. 1994, *ApJ*, 427, 784
- Shull, J. M., Smith, B. D., & Danforth, C. W. 2012, *ApJ*, 759, 23
- Smith, B. D., Hallman, E. J., Shull, J. M., & O'Shea, B. W. 2011, *ApJ*, 731, 6
- Spitler, L. G., Scholtz, P., Hessels, J. W. T., et al. 2016, *Nature*, 531, 202
- Taylor, J. H., & Cordes, J. M. 1993, *ApJ*, 411, 674
- Tendulkar, S. P., Bassa, C. G., Cordes, J. M., et al. 2017, *ApJ*, 843, L7
- Tepper-Garcia, T., Richter, P., Schaye, J., et al. 2012, *MNRAS*, 425, 1640
- Thornton, D., Stappers, B., Bates, S. D., et al. 2013, *Science*, 341, 53
- Tumlinson, J., Thom, C., Werk, J. K., et al. 2011, *Science*, 334, 948
- Wakker, B. D., Howk, J. C., Savage, B. D., et al. 1999, *Nature*, 402, 388
- Wang, X. D., Yao, Y., Tripp, T.M., et al. 2005, *ApJ*, 635, 386
- Yao, J. M., Manchester, R. N., & Wang, N. 2017, *ApJ*, 835, 29
- Yao, Y., & Wang, X. D. 2005, *ApJ*, 624, 751

TABLE 1
Redshift Estimates from FRB Dispersions^a

No.	FRB	DM_{obs} (cm^{-3} pc)	DM_{Gal} (cm^{-3} pc)	DM_{IGM} (cm^{-3} pc)	z_{Yao} (Model)	z_{SD} (Model)
1	FRB 121102	557 ± 2	287	170	0.238	$0.254^{+0.043}_{-0.032}$
2	FRB 010724	375 ± 3	32.7	181	0.254	$0.268^{+0.044}_{-0.033}$
3	FRB 130628	470 ± 1	47.0	323	0.453	$0.434^{+0.069}_{-0.052}$
4	FRB 010621	745 ± 10	321.6	323	0.453	$0.435^{+0.069}_{-0.052}$
5	FRB 150418	776 ± 5	325.5	351	0.492	$0.437^{+0.069}_{-0.052}$
6	FRB 120127	553 ± 3	20.6	432	0.607	$0.549^{+0.084}_{-0.063}$
7	FRB 140514	563 ± 6	24.2	438	0.615	$0.555^{+0.085}_{-0.064}$
8	FRB 131014	779 ± 1	220.2	459	0.643	$0.575^{+0.088}_{-0.066}$
9	FRB 110523	623 ± 6	33.0	490	0.687	$0.605^{+0.092}_{-0.069}$
10	FRB 110627	723 ± 3	33.6	589	0.826	$0.698^{+0.104}_{-0.079}$
11	FRB 101125	790 ± 3	75.9	614	0.861	$0.721^{+0.107}_{-0.081}$
12	FRB 130729	861 ± 2	25.4	736	1.031	$0.827^{+0.121}_{-0.091}$
13	FRB 090625	900 ± 1	25.5	774	1.085	$0.859^{+0.126}_{-0.095}$
14	FRB 130626	952 ± 1	65.1	787	1.104	$0.870^{+0.127}_{-0.096}$
15	FRB 110220	944 ± 5	24.1	820	1.150	$0.897^{+0.131}_{-0.098}$
16	FRB 110703	1104 ± 7	23.1	981	1.375	$1.025^{+0.148}_{-0.111}$
17	FRB 121002	1629 ± 2	60.5	1469	2.059	$1.380^{+0.196}_{-0.147}$
18	FRB 150610	1593.9 ± 0.6	122	1372	1.2	$1.313^{+0.187}_{-0.140}$
19	FRB 151206	1909.8 ± 0.6	16	1650	1.5	$1.502^{+0.212}_{-0.160}$
20	FRB 151230	960.4 ± 0.5	38	822	0.8	$0.899^{+0.131}_{-0.099}$
21	FRB 160102	2596.1 ± 0.3	13	2483	2.1	$2.018^{+0.283}_{-0.212}$
22	FRB 170107	609.5 ± 5	27	483	...	$0.598^{+0.091}_{-0.069}$
23	FRB 160317	1165 ± 11	395	670	0.7	$0.770^{+0.114}_{-0.086}$
24	FRB 160410	278 ± 3	62.5	115	0.2	$0.180^{+0.032}_{-0.023}$
25	FRB 160608	682 ± 7	310	272	0.4	$0.377^{+0.066}_{-0.045}$

^a Observed and IGM dispersion measures, DM_{obs} and DM_{IGM} , for 17 FRBs (Petroff et al. 2016; Yao et al. 2017) listed in order (#1 - #17) of increasing IGM dispersion and estimated redshift. The next 8 FRBs are taken from recent papers: #18 - #21 (Bhandari et al. 2017); #22 (Bannister et al. 2017); #23 - #25 (Caleb et al. 2017). Column 5 gives the IGM dispersion, after subtracting contributions from the Milky Way Galaxy (column 4) and FRB host galaxy (constant $100 \text{ cm}^{-3} \text{ pc}$). Column (6) gives estimated redshift quoted by Yao et al. (2017) and other groups. Column (7) gives our estimate of the redshift using equations [6] and [7] with $h_{70} = 1$ and baryon fraction $f_{\text{IGM}} = 0.6 \pm 0.1$. Errors on redshift do not include systematic effects from cosmological model (about 1%) or DM subtractions for Milky Way and FRB host galaxy (see discussion in Section 2.3).